Simulation and numerical analysis of pneumatic actuator behavior

Jakub Javorik

***Abstract*—**Goal of the work is to analyze the function of the pneumatic actuator. A relation between the device construction and the hysteresis in the pressure/stroke relation was studied. A Numerical model of the actuator was created and its results were analyzed. Hyperelastic material properties of the rubber diaphragm were applied in the model and influence of friction between rubber and steel parts of the actuator was evaluated. Reasons of hysteresis were identified and some modifications of the actuator are suggested.

***Keywords*—**hyperelasticity, hysteresis, numerical analysis, pneumatic actuator.

I. Introduction

THE paper deals with the numerical analysis of the mechanical behavior of the pneumatic actuator. High precision of control rod stroke is required for this important control and regulating device. Unfortunately, there is one negative effect, which affects the accuracy significantly. It is hysteresis in the stroke/pressure relation, i.e. difference in this relation during the pressure increase and decrease. This work analyzes the possible causes of this hysteresis, and searches a way to reduce it to a minimum.

Analysis will reveal only the reasons caused by the shape and assembly of the actuator, and by the friction between its particular parts. Others reasons as a possible viscoelastic behavior of the elastomer parts are not included.

II. Material and Methods

A. Actuator Geometry

The geometric model of the actuator is shown in Fig. 1 and the scheme of the actuator parts can be seen in Fig. 2. The elastic (rubber) diaphragm (a) is fixed between two discs (b) in the closed case (c) and it is mounted on a steel core (d). This core is supported by the steel spring (e) on the one side. A control rod is connected with this assembly. The rubber diaphragm is reinforced by the textile on one side (f).

A pressure difference on the one and the other side of the diaphragm causes movement of the rod in the axial direction of the actuator.

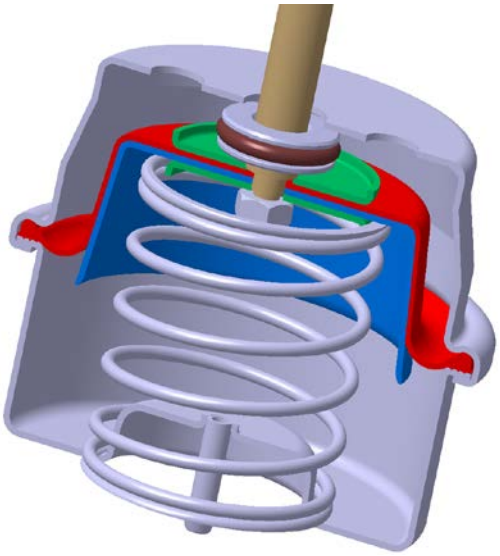

Fig. 1 partially cut model of the actuator

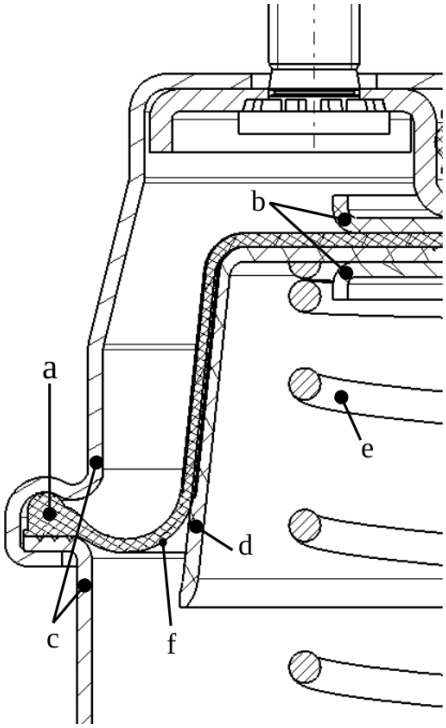

Fig. 2 scheme of the actuator structure

J. Javorik is with the Tomas Bata University in Zlin, nam. T. G. Masaryka 5555, 760 01 Zlin, Czech Republic (phone: +420 576 035 151; fax: +420 576 035 176; e-mail: javorik@ft.utb.cz).

B. Material Characterization

Basic element of the actuator is the rubber diaphragm (Fig. 2a). Final position of the control rod depends on the mechanical properties of the diaphragm, on the spring stiffness (Fig. 2e), and on the pressure difference inside the actuator.

Therefore we need to characterize the mechanics of the rubber diaphragm accurately. Due to these facts, the material of the diaphragm (elastomer) was tested in all three basic deformation modes (Fig. 3): uniaxial tension (Fig. 3a), equibiaxial tension (Fig. 3b) and pure shear (Fig. 3c). Data from these tests are needed to set correct constants for hyperelastic material model [1]-[8]. The properties of textile were measured in uniaxial tension test.

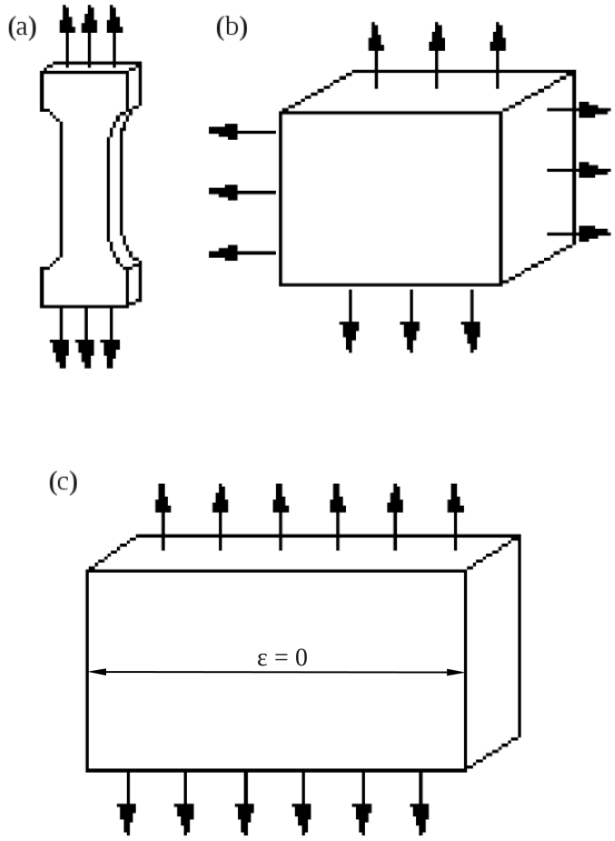

Fig. 3 schemes of three deformation modes of elastomer tests

Uniaxial tension test of textile

Textile of the diaphragm was tested in uniaxial tension test, to find out basic mechanical constants of this material. Young modulus (in warp direction) and Poisson ratio were evaluated in this test.

Uniaxial tension test of elastomer

Uniaxial tension tests of elastomer [9], according ISO 37 standard, was performed to determine the hyperelastic material parameters. The test was performed on a universal tensile testing machine. A 1 mm thick dumb-bell shaped specimen (type 1A – ISO 37) was used (Fig. 4). Stress/strain curve was measured during the whole range of loading. Specimens were loaded up to deformation of ε=1.0.

Fig. 4 1A type of uniaxial tension test specimen (ISO 37)

Equibiaxial tension test of elastomer

A bubble inflation technique was used to characterize the elastomer in the equibiaxial tension [10]-[15].

The bubble inflation technique involves a uniform circular specimen clamped at the rim and inflated by increasing the air pressure on one side. The specimen deforms into the shape of bubble (Fig. 5 and 6). The inflation of the specimen results in an equibiaxial stretching near the pole of the bubble and a planar tension near the rim. Due to the spherical symmetry at the bubble pole, where σ represents the hoop stress $\sigma_{\theta\theta}=\sigma_{\varphi\varphi}$. Then the Cauchy stress tensor can be expressed as

$$\sigma = \begin{bmatrix} \sigma_{rr} & 0 & 0 \\ 0 & \sigma_{\theta\theta} & 0 \\ 0 & 0 & \sigma_{\theta\theta} \end{bmatrix}. \quad (1)$$

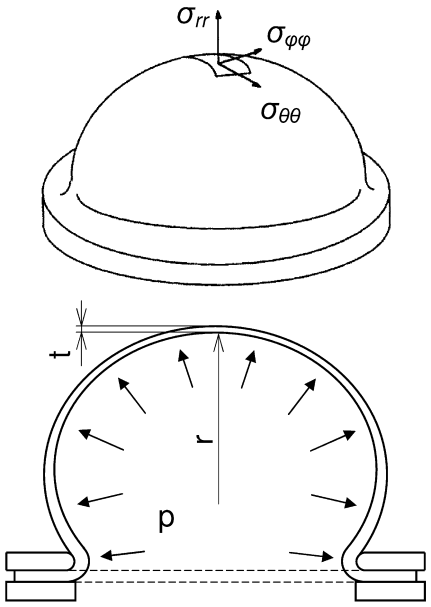

Fig. 5 the bubble inflation technique

As the thickness t of the inflated specimen is small compared with its radius of curvature r, the thin shell assumption is appropriate, allowing us to neglect the radial stress σ_{rr} in comparison with the stress $\sigma_{\theta\theta}$. In addition we equate $\sigma_{\theta\theta}$ to the thickness-averaged hoop stress, which leads to

$$\sigma_{\theta\theta} = \frac{pr}{2t}, \tag{2}$$

where p is the differential inflation pressure inside the bubble, r is radius of curvature of the specimen and t is the specimen thickness (Fig. 5).

Considering the material incompressibility, the thickness of the inflated specimen can be expressed as

$$t = \frac{t_0}{\lambda_{\theta\theta}^{\ 2}}, \tag{3}$$

where t_0 is the initial specimen thickness (unloaded state). The stretch $\lambda_{\theta\theta}$ at the pole of the inflated specimen must be measured. Generally, the stretch λ is the ratio between the actual length l and the initial length l_0, or

$$\lambda = \frac{l}{l_0}. \tag{4}$$

Using a video camera, the stretch $\lambda_{\theta\theta}$ and the radius of curvature r were measured.

Substituting equation (3) into the equation (2) the hoop stress becomes

$$\sigma_{\theta\theta} = \frac{pr\lambda_{\theta\theta}^{\ 2}}{2t_0}. \tag{5}$$

To compute the hoop stress $\sigma_{\theta\theta}$ from the (5) the pressure p inside the bubble, the radius of curvature of the bubble r, and the stretch $\lambda_{\theta\theta}$ at the bubble pole must be measured during the inflation. To characterize the hyperelastic material behavior, knowledge of the entire stress/strain curve is necessary (Fig. 7). Thus, the above mentioned parameters were recorded continuously during the whole test.

Fig. 6 inflated equibiaxial specimen with white stripes

Specimens with thickness t_0=1 mm were tested, and diameter of the hole through which the bubble is inflated was 50 mm. Pressure was measured using a digital manometer. The inflation of the specimen was recorded using a video camera and the stretch and bubble radius were obtained by analyzing the resulting video. Finally, the manometer display appeared in the video images, so relating the pressure to every stretch or radius value was simple and reliable.

To determine the bubble radius and stretch from the video images, two stripes were drawn on the specimen surface, identifying two points on the bubble silhouette. Tracing an arc through these points and the pole of the bubble allows the determination of the radius and the length of the arc (Fig. 6).

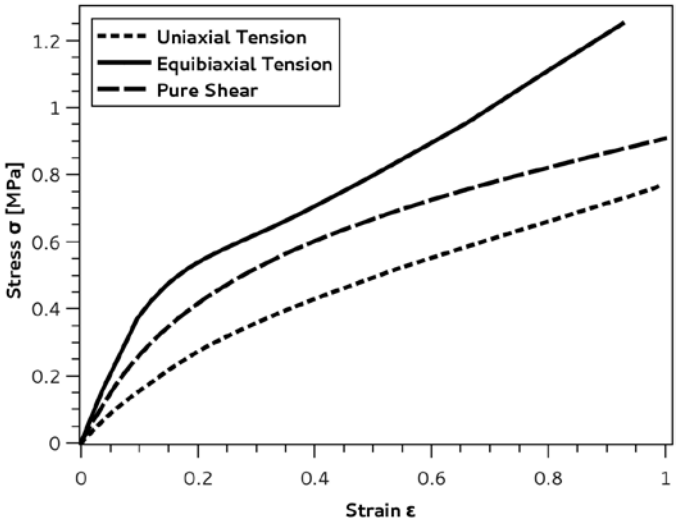

Fig. 7 results of tests of elastomer

Pure shear test of elastomer

In this test, the specimen is loaded by tension similarly like in the uniaxial tension test. Important difference is in the boundary conditions during the test. Cross-section area of the uniaxial specimen (Fig. 3a) is not constrained and it can freely contract in its both dimensions during the loading. Contrary uniaxial tension, pure shear specimen can change only its thickness during the test. Its width will remain constant during the whole range of loading (Fig. 3c). To fulfill this condition it is necessary that the height of the sample is substantially smaller than its width and that both longitudinal edges of specimen are firmly clamped in the long clamps which prevent change of the specimen width.

C. Hyperelasticity

A hyperelastic material constants will be set up from results of tests presented above. Currently, a number of hyperelastic material models are available that vary in defining the strain energy density function W [16]-[21]. W is a function of a deformation tensor, whose derivative with respect to a strain component determines the corresponding stress component. Explicitly,

$$S_{ij} = \frac{\partial W}{\partial C_{ij}}, \tag{6}$$

where S_{ij} are components of the 2nd Piola Kirchhoff stress tensor and C_{ij} are components of the right Cauchy-Green deformation tensor [22], which will be as follows

$$C_{ij} = \begin{bmatrix} \lambda_1^{\,2} & 0 & 0 \\ 0 & \lambda_2^{\,2} & 0 \\ 0 & 0 & \lambda_3^{\,2} \end{bmatrix}. \quad (7)$$

Hyperelastic models are usually named after their authors. Some of the best known and most used models are: Neo-Hookean, Mooney-Rivlin, Yeoh, Second Order Invariant, James-Green-Simpson, Ogden, Gent, Arruda-Boyce [23]-[28].

D. Numerical (FEM) Model of the Actuator

Considering the geometry of actuator (Fig. 1 and 2), the finite element (FE) numerical model was created (Fig. 8) [29]-[47]. Thanks to the axial symmetry of the whole problem we could make 2D axisymmetric model with defined axis of symmetry. The model consists of planar surface which represents half section of the elastic diaphragm, then of three curves that represent rigid parts of the assembly, and of central element (lower straight line) that represents elastic support (spring) (Fig. 8). This element is located in the axis of symmetry of the actuator.

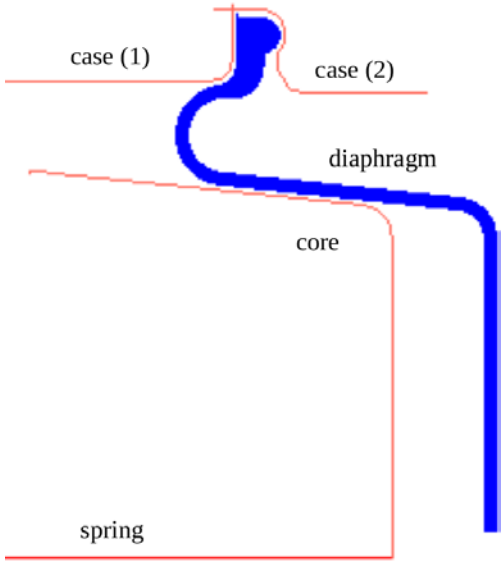

Fig. 8 numerical finite element model of the actuator

The diaphragm consists of two materials: elastomer which is joined with textile from one side. The textile (Fig. 2f) is on the side where the diaphragm is in contact with the metal core of the actuator (Fig. 2). Material parameters of textile were measured in uniaxial tension test and they are: Young modulus E=280 MPa (and no bending stiffness, i.e. no rotation degrees of freedom are shared) and the Poisson ratio v=0.3. From hyperelastic tests of elastomer (mentioned in the chapter II.B) Arruda-Boyce hyperelastic model was set for elastomer [48]. To set up hyperelastic material constants of this model, least square method was used. Constants were computed from the data shown in Fig. 7 and 9. Comparison of the Arruda-Boyce hyperelastic model and experimental data is in Fig. 9.

Arruda-Boyce hyperelastic model defines strain energy density function W as

$$W = \mu \sum_{i=1}^{5} \frac{c_i}{\lambda_L^{\,2i-2}} \left(I_1^{\,i} - 3^i \right), \quad (8)$$

where I_1 is first invariant of the right Cauchy-Green deformation tensor, defined in (7), and the constants c_i are always defined as: c_1 = 1/2, c_2 = 1/20, c_3 = 11/1050, c_4 = 19/7000 and c_5 = 519/673750. Initial shear modulus μ and limiting stretch λ_L are hyperelastic constants computed from experimental data. Constants computed for the model shown in Fig. 9 are: μ=0.38793 MPa and λ_L=995567.

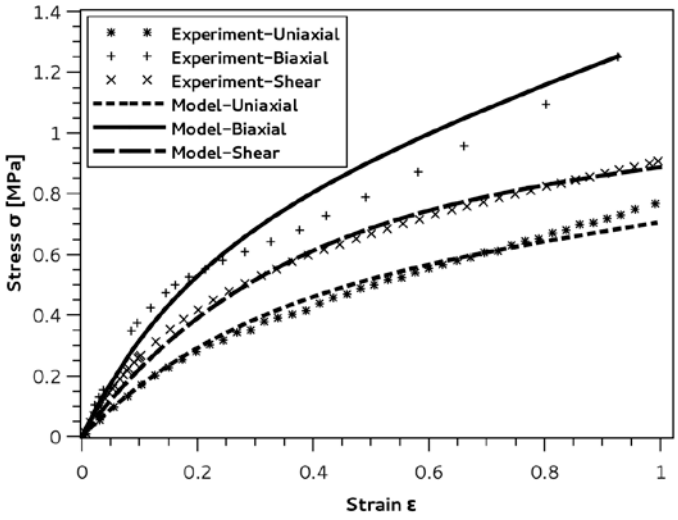

Fig. 9 fitting of hyperelastic model and experimental data

Curves of both parts of actuator case and core (Fig. 8) are created as rigid bodies. Central spring stiffness is 3 N/mm. A contact between rigid parts of the model and the elastic diaphragm was defined in the model.

E. Loads and Boundary Conditions of Numerical Model

Whole analysis consists of four basic steps:

- clamping the outer rim of the diaphragm in the actuator case (time: 0.0 to 1.0),
- mounting the diaphragm on the core (time: 1.0 to 2.0),
- pressure decreasing on the left side of the diaphragm (time: 2.0 to 3.0),
- returning the pressure to its initial value (time: 3.0 to 4.0).

Clamping of the Diaphragm Rim in the Actuator Case

As we need to be as close to the reality as it is possible, the fixation of the diaphragm in the model is done by real clamping of the diaphragm rim between two parts of the

actuator case (Fig. 10). A contact between the case parts and the diaphragm is applied and the two parts of the case approach against each other.

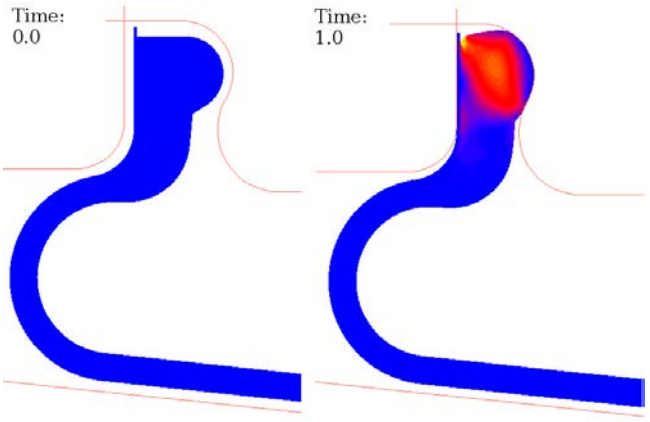

Fig. 10 clamping of the diaphragm rim in the actuator

Mounting the Diaphragm on the Core

The steel core (with the spring element) is pushed into the diaphragm during the second step (Fig. 11). The contact between the core and the diaphragm occurs and the initial position of actuator parts, before the pressure application, is reached.

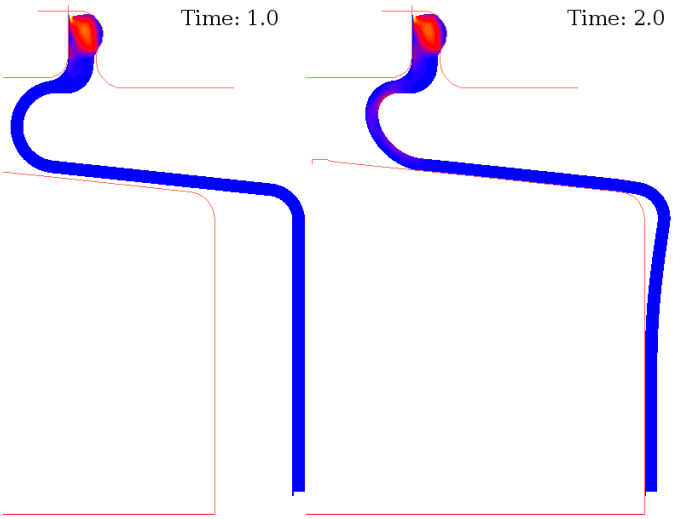

Fig. 11 mounting the diaphragm on the core

Pressure Application on One Side of the Diaphragm

Left end of the spring is fixed at the beginning of this step and the pressure decrease is applied on the inner (left) side of the diaphragm (side with the textile). The spring is pressed by this condition and the core moves to left in the Fig. 12.

Returning the Pressure to Its Initial Value

The fourth step is opposite to the third step. The pressure increases to the initial value and the core with the diaphragm return to the same position as at time=2.0.

For the analysis of the influence of friction a number of friction coefficients were used. Computations were carried out with next friction coefficients (f_c): 0; 0.05; 0.07; 0.1; 0.15; 0.25 and 0.35.

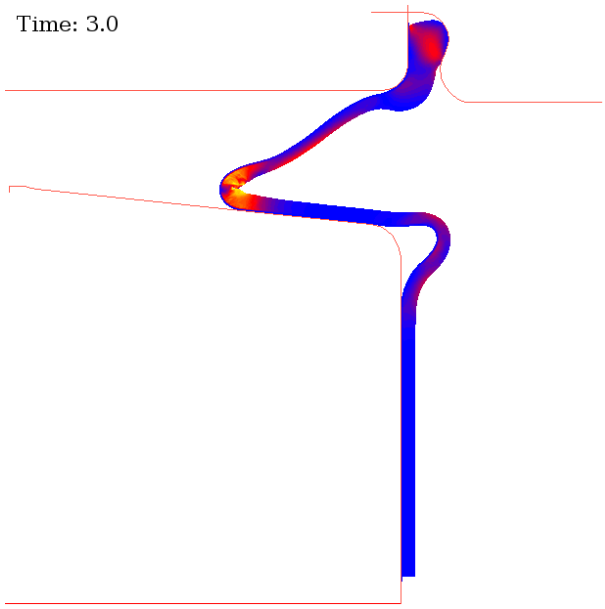

Fig. 12 model after the application of pressure

III. Results and Discussion

Two main effects were evaluated. If, and how could the friction influence the stroke/pressure hysteresis? Stroke was measured as a horizontal displacement of the actuator core. And secondly influence of diaphragm structure and geometry on its deformation and on the hysteresis was studied.

A. Influence of Friction on the Hysteresis

The largest hysteresis occurred in the models with friction coefficient f_c = 0.05 and f_c = 0.07. The situation in these two cases is the same and the result is shown in the Fig. 13. The hysteresis is decreasing with a next increase or decrease of the value of friction coefficient and it will vanish when the friction coefficient has value f_c = 0 or its value is higher than 0.25 (Table I and Fig. 14).

During loading and movement of the diaphragm, it tends to slip over the surface of the core, and this fact causes a rising of the diaphragm edge from the core edge (Fig. 15). Then the hysteresis is caused by a difference between moments in which the slip occurs, because the moments of these slips can differ in case of pressure decreasing and pressure increasing. If the friction coefficient f_c = 0, the slip should occur in the same moment without the influence of a previous history of loading (decrease or increase of pressure) and thus no hysteresis should occur. This fact was also approved by the results of the model with f_c = 0. This model was therefore used to approve initial hypothesis about the fact that the only the friction will be the reason of the hysteresis in the numerical model.

Results, described above, shows that the pressure will not always be sufficient to fix the diaphragm to the core surface and then the slip of the diaphragm can occur. Thus some modification in shape and dimension of particular parts of actuator (for example large radius of the upper disc (b) in Fig. 2) could solve this problem.

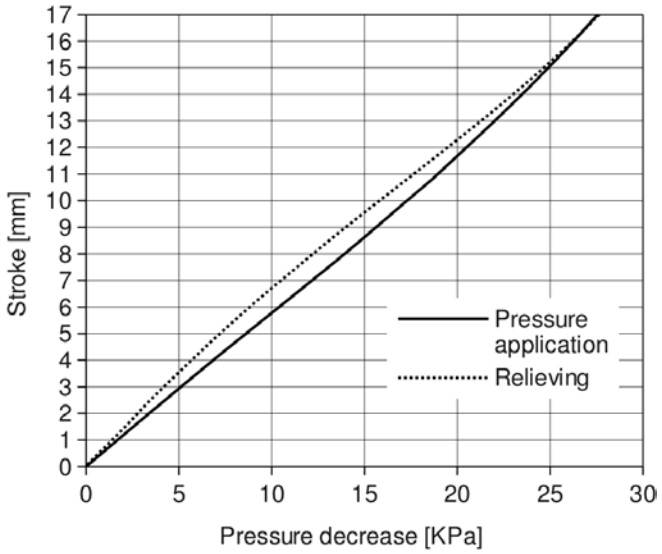

Fig. 13 hysteresis in the pressure/stroke relation with the friction coefficients 0.05 and 0.07

TABLE I INFLUENCE OF FRICTION COEFFICIENT ON THE HYSTERESIS IN NUMERICAL MODEL

Friction coefficient f_c	Hysteresis [mm]
0	0
0.05	0.76
0.07	0.783
0.1	0.285
0.15	0.174
0.25	0.046
0.35	0

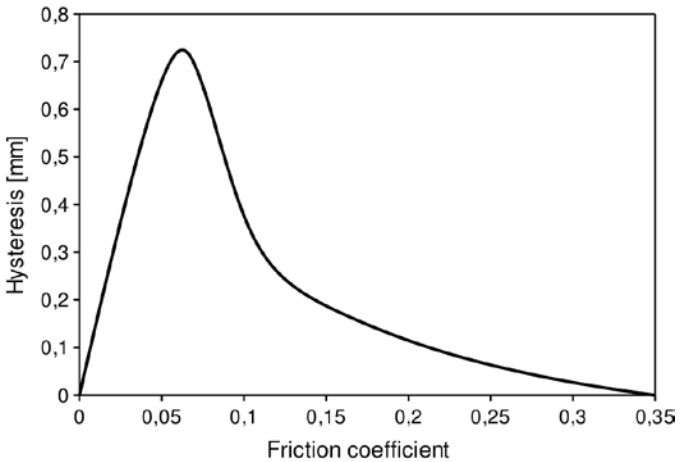

Fig. 14 relation between the friction and the hysteresis

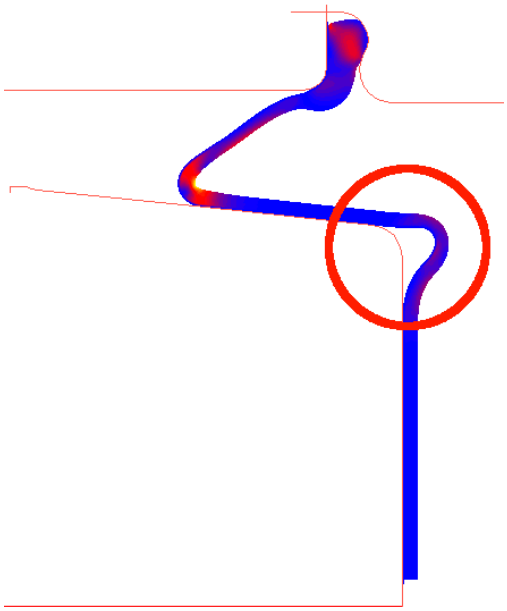

Fig. 15 the diaphragm edge raising during the pressure change

The maximal values of hysteresis in numerical models with f_c = 0.05 and f_c = 0.07 are 0.76 mm and 0.78 mm respectively (Table I). We can compare the results of model shown in Fig. 13 with the results of tests of real actuators in Fig. 16. Five actuators were tested and average hysteresis was 1.21 mm (Table II).

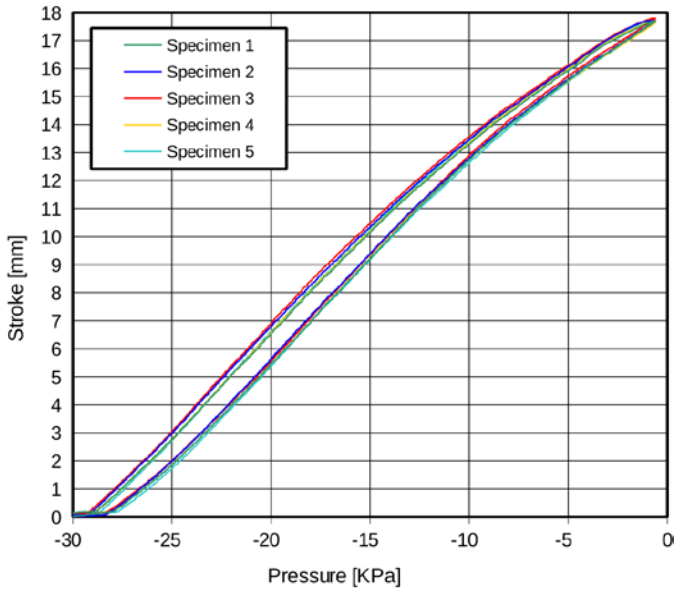

Fig. 16 results of tests of real actuators

We can see that the real hysteresis is larger then the hysteresis computed in numerical model. It means that apart form the friction there are other factors influencing the hysteresis. But these factors were not included in the

numerical model because our main goal was to find out how the friction influences the hysteresis. The most significant of these other factors will be the own hysteresis of elastomer which is generally known and described [49]. To be sure about the elastomer hysteresis a cyclic tension test of the elastomer was carried out. On the results of this test (Fig. 17) we can clearly see the hysteresis of the material and even the Mullins effect [50]-[54].

TABLE II HYSTERESIS IN REAL ACTUATORS

Specimen number	Hysteresis [mm]
1	1.13
2	1.22
3	1.38
4	1.02
5	1.28
Average hysteresis	**1.21**

B. Influence of Diaphragm Structure on Its Deformation

The bend of diaphragm, which occurs when the diaphragm is rolling on the surface of the core, is a next critical point. The maximum of stress and strain occurs here (Fig. 18).

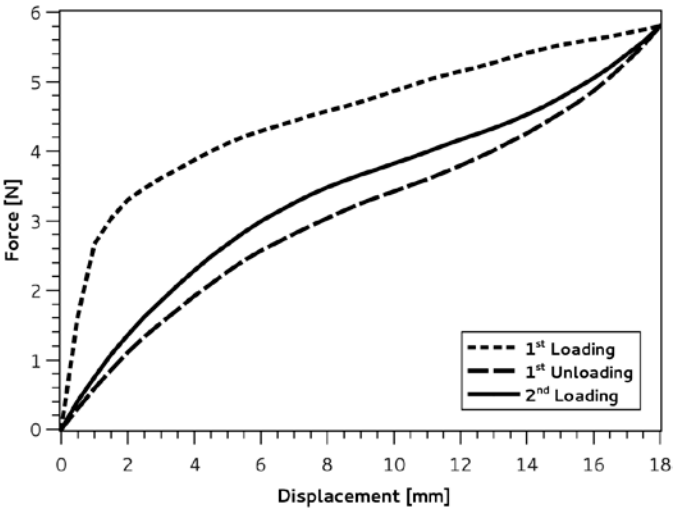

Fig. 17 result of cyclic tension test of diaphragm elastomer

The textile tension stiffness is significantly greater than the stiffness of the diaphragm elastomer. Thus, only the compression occurs in the entire thickness of the elastomer during the diaphragm bending shown in Fig. 18 and 19. Due to that fact a collapse of the diaphragm can occur at the end of stroke and a self contact of the diaphragm surface should occur (Fig. 19).

Therefore, there is a contact between the two faces of the diaphragm. In this case, there would be a considerably greater friction than in the case of contact of the diaphragm (from the side with textile) with a steel core. That phenomenon could again strongly affect the hysteresis.

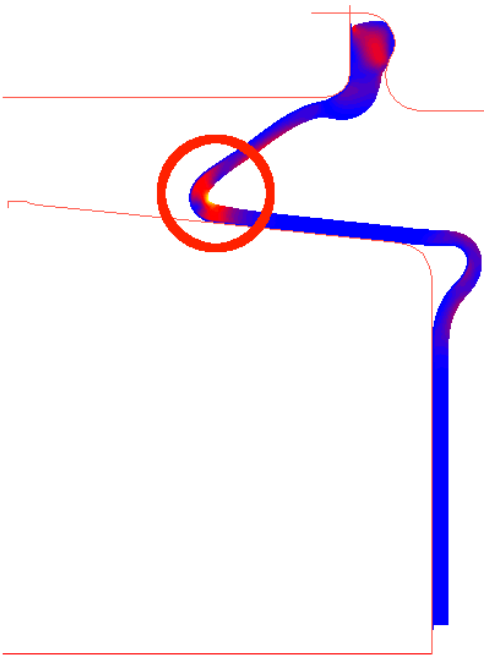

Fig. 18 critical point of model where the maximum of stress and strain occurs

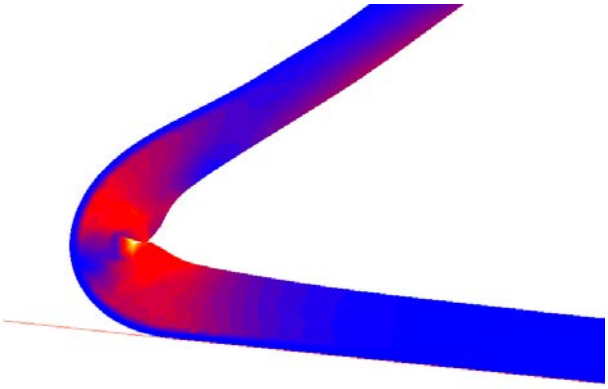

Fig. 19 the diaphragm collapse during its rolling on the core

IV. CONCLUSION

Possible critical effects were revealed in the actuator analysis. They are: diaphragm slipping on the core surface and diaphragm collapse during the rolling along the core. These facts should be considered during future designs and modifications of actuators. Next possible effects as for example a viscoelastic character of elastomer, which were not included in the model, could increase the hysteresis of the real actuator.

REFERENCES

[1] R. W. Ogden, *Non-linear Elastic Deformations*. New York: Dover Publications, 1997.
[2] A. N. Gent, *Engineering with Rubber*. Munich: Hanser, 2001.
[3] N. Huber, and C. Tsakmakis, "Finite deformation viscoelasticity laws," *Mech. Mater.*, vol. 32, pp. 1-18, 2000.

[4] A. N. Gent, "Extensibility of rubber under different types of deformation," *J. Rheol.*, vol. 49, pp. 271–275, 2005.

[5] L. R. G. Treloar, "Mechanics of rubber elasticity," *J. Polym. Sci. Pol. Symp.*, vol. 48, pp. 107–123, 1974.

[6] L. R. G. Treloar, *The Physics of Rubber Elasticity*. Oxford: Clarendon Press, 1975.

[7] R. H. Finney, and A. Kumar, "Development of material constants for nonlinear finite element analysis," *Rubber Chem. Technol.*, vol. 61, pp. 879–891, 1988.

[8] O. H. Yeoh, "Characterization of elastic properties of carbon black filled rubber vulcanizates," *Rubber Chem. Technol.*, vol. 63, pp. 792-805, 1990.

[9] L. P. Smith, *The Language of Rubber*. Oxford: Butterworth-Heinemann, 1993.

[10] J. Javorik, and Z. Dvorak, "Equibiaxial test of elastomers," *KGK-Kautsch. Gummi Kunstst.*, vol. 60, pp. 608-610, 2007.

[11] W. D. Kim, W. S. Kim, C. S. Woo, and H. J. Lee, "Some considerations on mechanical testing methods of rubbery materials using nonlinear finite element analysis," *Polym. Int.*, vol. 53, pp. 850–856, 2004.

[12] L. Chevalier, and Y. Marco, "Tools for multiaxial validation of behavior lows chosen for modeling hyperelasticity of rubber-like materials," *Polym. Eng. Sci.*, vol. 42, pp. 280-298, 2002.

[13] N. Reuge, F. M. Schmidt, Y. Le Maoult, M. Rachik, and F. Abbe, "Elastomer biaxial characterization using bubble inflation technique. I: Experimental investigations," *Polym. Eng. Sci.*, vol. 41, pp. 522-531, 2001.

[14] J. Javorik, and Z. Dvorak, "The testing of hyperelastic properties of the rubber materials," *Chem. Listy*, vol. 105, pp. 273-274, 2011.

[15] J. E. Mark, "Some unusual elastomers and experiments on rubberlike elasticity," *Prog. Polym. Sci.*, vol. 28, pp. 1205-1221, 2003.

[16] R. S. Rivlin, and K. N. Sawyers, "Strain-energy function for elastomers," *Tran. Soc. Rheol.*, vol. 20, pp. 545–557, 1976.

[17] M. H. B. M. Shariff, "Strain energy function for filled and unfilled rubberlike material," *Rubber Chem. Technol.*,, vol. 73, pp. 1–21, 2000.

[18] G. A. Holzapfel, *Nonlinear Solid Mechanics*. Chichester: Wiley, 2000.

[19] M. Bercovier, E. Jankovich, F. Leblanc, and M. A. Durand, "A finite element method for the analysis of rubber parts: Experimental and analytical assessment," *Comput. Struct.*, vol. 14, pp. 384-391, 1981.

[20] J. E. Mark, B. Erman, and F. R. Eirich, *Science and Technology of Rubber*. New York: Academic Press, 1994.

[21] A. Boukamel, L. Laiarinandrasana, S. Méo, and E. Verron, *Constitutive Models for Rubber V*. London: Taylor & Francis, 2008.

[22] A. F. Bower, *Applied Mechanics of Solids*. New York: CRC Press, 2009.

[23] P. Haupt, and A. Lion, "On finite linear viscoelasticity of incompressible isotropic materials," *Acta Mech.*, vol. 159, pp. 87–124, 2002.

[24] A. N. Gent, "A new constitutive relation for rubber," *Rubber Chem. Technol.*, vol. 69, pp. 781-785, 2001.

[25] R. S. Rivlin, "Finite elasticity theory as a model in the mechanics of viscoelastic materials," *J. Polym. Sci. Pol. Symp.*, vol. 48, pp. 125-144, 1974.

[26] O. H. Yeoh, "Some forms of the strain energy function for rubber," *Rubber Chem. Technol.*, vol. 66, pp. 754-771, 1993.

[27] R. A. Brockman, "On the use of the Blatz-Ko constitutive model for nonlinear finite element analysis," *Comput. Struct.*, vol. 24, pp. 607–611, 1986.

[28] M. C. Boyce, "Direct comparison of the Gent and the Arruda-Boyce constitutive models of the rubber elasticity," *Rubber Chem. Technol.*, vol. 69, pp. 781–785, 1996.

[29] J. Javorik, and M. Stanek, "The shape optimization of the pneumatic valve diaphragm," *Int. J. Math. Comput. Simul.*, vol. 5, pp. 361–369, 2011.

[30] J. Javorik, and M. Stanek, "The numerical simulation of the rubber diaphragm behavior," in *Recent Res. in Autom. Control : 13th WSEAS Int. Conf. on Autom. Control, Modell. & Simul.*, Lanzarote, Spain: WSEAS Press, 2011, pp. 117–120.

[31] L. J. Billings, and R. Shepherd, "The modeling of layered steel/elastomer seismic base isolation bearings," in *Proc. 1992 MARC User Conf.*, Monterey, CA, USA, 1992.

[32] M. C. Popescu, and M. E. Mastorakis, "Optimal flow control of a three tank system," *Int. J. of Math. Comput. in Simul.*, vol. 3, pp. 179-186, 2009.

[33] A. Arghiropol, and C. Rotaru, "Overview of the 2D and 3D finite element studies versus experimental results of a solid propellant engine performances under cycling loading effect," *Int. J. of Math. Comput. in Simul.*, vol. 4, pp. 42-49, 2010.

[34] S. Amornsamankul, K. Kaorapapong, and B. Wiwatanapataphee, "Three-dimensional simulation of femur bone and implant in femoral canal using finite element method," *Int. J. of Math. Comput. in Simul.*, issue 4, vol. 4, pp. 171-178, 2010.

[35] O. Suba, and L. Sykorova, "Transient of thermal stresses in printed circuit boards," *Int. J. Mech.*, vol. 5, pp. 226–233, 2011.

[36] L. Sykorova, and O. Suba, "The transient temperature field simulation of polymeric materials during laser machining," *Int. J. Mech.*, vol. 5, pp. 234–241, 2011.

[37] M. Stanek, D. Manas, M. Manas, and O. Suba, "Optimization of injection molding process," *Int. J. Math. Comput. Simul.*, vol. 5, pp. 413–421, 2011.

[38] M. Stanek, D. Manas, M. Manas, and J. Javorik, "Simulation of injection molding process by Cadmould Rubber," *Int. J. Math. Comput. Simul.*, vol. 5, pp. 422–429, 2011.

[39] O. Suba, L. Sykorova, S. Sanda, and M. Stanek, "Modeling of thermal stress in printed circuit boards," in *Recent Res. in Autom. Control : 13th WSEAS Int. Conf. on Autom. Control, Modell. & Simul.*, Lanzarote, Spain: WSEAS Press, 2011, pp. 173-176.

[40] O. Suba, L. Sykorova, S. Sanda, and M. Stanek, "Stress-state modelling of injection-molded cylindrical bosses reinforced with short fibers," in *Recent Res. in Autom. Control : 13th WSEAS Int. Conf. on Autom. Control, Modell. & Simul.*, Lanzarote, Spain: WSEAS Press, 2011, pp. 177-179.

[41] L. Sykorova, O. Suba, M. Malachova, and J. Cerny, "Temperature field simulation of polymeric materials during laser machining using COSMOS/M software," in *Recent Res. in Autom. Control : 13th WSEAS Int. Conf. on Autom. Control, Modell. & Simul.*, Lanzarote, Spain: WSEAS Press, 2011, pp. 180-184.

[42] M. Stanek, D. Manas, M. Manas, and J. Javorik, "Simulation of injection molding process," in *Recent Res. in Autom. Control : 13th WSEAS Int. Conf. on Autom. Control, Modell. & Simul.*, Lanzarote, Spain: WSEAS Press, 2011, pp. 231-234.

[43] M. Stanek, D. Manas, M. Manas, and O. Suba, "Optimization of injection molding process by MPX," in *Recent Res. in Autom. Control : 13th WSEAS Int. Conf. on Autom. Control, Modell. & Simul.*, Lanzarote, Spain: WSEAS Press, 2011, pp. 212-216.

[44] M. S. Salleh, M. Z. Omar, J. Syarif, M. N. Mohammed, and K. S. Alhawari, "Thermodynamic simulation on thixoformability of aluminium alloys for semi-solid metal processing," *Int. J. of Math. Comput. in Simul.*, vol. 7, pp. 286–293, 2013.

[45] D. Samek, and J. Javorik, "Numerical analysis of shape stability of rubber boot," *Int. J. Mech.*, vol. 7, pp. 293-301, 2013.

[46] A. Ionescu, M. Calbureanu, and M. Negru, "Static and dynamic simulation in the seismic behavior of a building structure using ANSYS program," *Int. J. Mech.*, vol. 7, pp. 210-217, 2013.

[47] K. Frydrysek, R. Janco, and H. Gondek, "Solutions of beams, frames and 3D structures on elastic foundation using FEM," *Int. J. Mech.*, vol. 7, pp. 362-369, 2013.

[48] E. M. Arruda, and M. C. Boyce, "A three-dimensional constitutive model for the large stretch behavior of rubber elastic materials," *J. Mech. Phys. Solids* , vol. 41, pp. 389-412, 1993.

[49] J. E. Mark, "Rubber elasticity," *Rubber Chem. Technol.*, vol. 55, pp. 1123–1136, 1982.

[50] L. Mullins, "Softening of rubber by deformation," *Rubber Chem. Technol.*, vol. 42, pp. 339-362, 1969.

[51] S. Govindjee, and J. C. Simo, "A micro-mechanically based continuum damage model for carbon black filled rubbers incorporating mullins' effect," *J. Mech. Phys. Solids*, vol. 39, pp. 89–112, 1991.

[52] A. Vandenbroucke, H. Laurent, N. Ait Hocine, and G. Rio, "Hyperelasto-visco-hysteresis model for an elastomeric behaviour: Experimental and numerical investigation," *Comput. Mater. Sci.*, vol. 48, pp. 495–503, 2010.

[53] L. M. Yang, and V. P. W. Shim, "A visco-hyperelastic constitutive description of elastomeric foam," *Int. J. Impact Eng.*, vol. 30, pp. 1099–1110, 2004.

[54] A. E. Zuniga, and M. F. Beatty, "A new phenomenological model for stress-softening in elastomers," *Z. Angew. Math. Phys.*, vol. 53, pp. 794–814, 2002.